Silicon MIT Virtual Source Model (VERSION=1.0.1)

Table of Contents

Microsystems Technology Laboratories, Massachusetts Institute of Technology, Cambridge, MA 02139

Terminals and Voltage Definitions

Figure 1 shows the MOSFET schematic where external terminals are labeled as **d** (drain), **g** (gate), **s** (source), **b** (body). Internal gate and body terminals are the same as the external ones. Internal drain terminal is labeled as **di**, while internal source terminal is labeled as **si**.

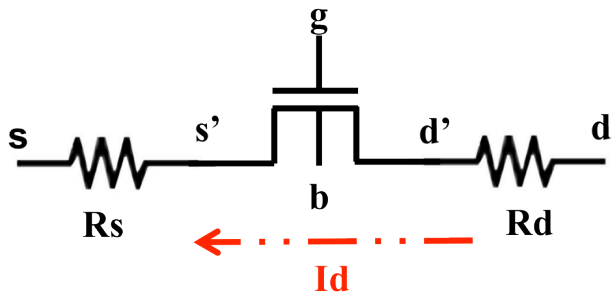

Figure 1: Schematic of the MOSFET with various terminals labeled. The current in the channel is labeled as Id. Id is positive when it flows from **d** to **s** terminal, while it is negative when it flows from **s** to **d** terminal.

Voltage definitions

Vds = tipe*|V(d)-V(s)|
Vgs = tipe*max(V(g)-V(s), V(g)-V(d))
Vgd = tipe*min(V(g)-V(s), V(g)-V(d))
Vbs = tipe*max(V(b)-V(s), V(b)-V(d))

Vdsi = tipe*|V(di)-V(di)|
Vgsi = tipe*max(V(g)-V(si), V(g)-V(di))
Vdgi = tipe*min(V(g)-V(si), V(g)-V(di))
Vbsi = tipe*max(V(g)-V(si), V(g)-V(di))

Vgs_raw = tipe*(V(g)-V(si))
Vgd_raw = tipe*(V(g)-V(di))

User-defined/extracted variables

The variables highlighted in blue are extracted upon calibration with experimental data as explained in section Parameter Extraction on pg. 14.

Table I: Variables and their meaning used in Si-MVS model.

Symbol	Meaning
tipe	type of transistor. nFET tipe=1; pFET tipe=-1
W	Transistor width [cm]
Lgdr	Physical gate length [cm]
dLg	Overlap length including both source and drain sides [cm].
Cg	Gate-to-channel areal capacitance at the virtual source [F/cm^2]
etov	Equivalent thickness of dielectric at S/D-G overlap [cm]
delta	Drain-induced-barrier-lowering (DIBL) [V/V]
n0	Subthreshold swing factor [unit-less] {typically between 1.0 and 2.0]
Rs0	Access resistance on terminal **s** [Ohms-micron]
Rd0	Access resistance on terminal **d** [Ohms-micron]
Cif	Inner fringing source or drain capacitance [F/cm]
Cof	Outer fringing capacitance [F/cm]
vxo	Virtual source carrier velocity [cm/s]
mu	Low-field carrier “apparent mobility” [cm^2/V.s]
beta	Saturation factor. Typ. ~ 1.8
Tjun	Junction temperature [K]
phib	Effective body voltage for Vt dependence on body bias. Typ. abs(2*phif)>0 [V]
gamma	Effective body factor. Typ. 0.1-1 except =0 for fully depleted FETs [sqrt(V)]
Vt0	Strong inversion threshold voltage at Vds = 0 V [V]
alpha	Empirical parameter associated with threshold voltage shift (in kT/q) between strong and weak inversion. Typ. =3.5 [unit-less]
mc	Carrier effective mass used for computation of charges for ballistic and blended quasi-ballistic model.
CTM_select	If CTM_select = 1, DD-NVSAT charge-transport model is selected, otherwise blended DD_NVSAT and ballistic charge-transport model is selected. Default is 1.
nd	Dependence of n on Vds [1/V]

Introduction

Silicon MIT virtual source (Si-MVS) model is a semi-empirical model that describes the short-channel metal-oxide-semiconductor-field-effect transistor (MOSFET) current versus voltage characteristics and is valid in all regions of operation with continuity of both current and its derivatives (Khakifirooz, Nayfeh et al. 2009). The model also provides intrinsic charge descriptions that extend all the way to the ballistic regime, where gradual channel approximation (GCA) is often violated. Rather than calculating all the inter-terminal capacitances separately from the transport model (Chan, Hui et al. 1998), the intrinsic charges associated with each terminal are calculated self consistently with the current model (Wei, Mysore et al. 2012). The MVS model maintains the advantage of using only a limited number of input parameters, most of which have straightforward physical meanings and can be easily measured from device characterization (Jeong, Antoniadis et al. 2009).

Drain current model

When devices are scaled to the deep sub-micrometer regime, carriers in the transistor channel (electrons or holes) experience fewer scattering events traveling along the channel (Lundstrom 2009). Depending on the channel length and material system of the transistor, devices may operate in quasi-ballistic (QB) transport regime as opposed to the drift-diffusive (DD) transport regime (Natori 1994), (Rhew, Ren et al. 2002).

The drain current in the MOSFET can be described by the product of the local charge areal density times the local carrier velocity at any point in the channel. It is particularly useful to write this expression at the location of the "virtual source" (VS), i.e. the location at the top of the energy barrier ($x = x_0$) as shown in Figure 2 since it is easiest to compute the charge density at the VS point.

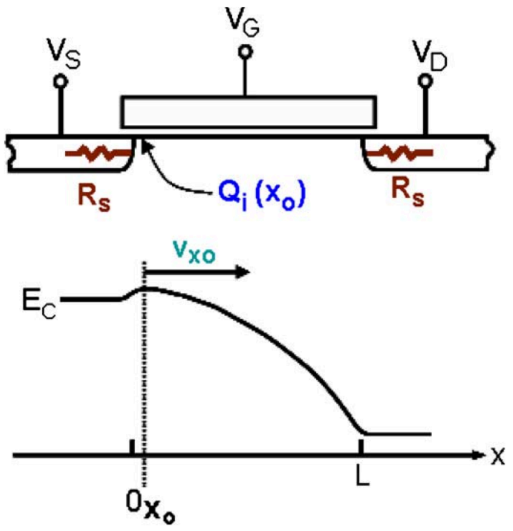

Figure 2: Schematic of a short-channel n-MOSFET with corresponding energy diagram. Virtual-source point x_0 is shown in the figure. The carrier charge and density used throughout this work are defined at this point (at the peak of the conduction band profile).

To model the transition from saturation to linear regime of transport, an empirical function, Fsat, is used. Hence, the current Id flowing from terminal **d** to terminal **s** (see Figure 1).

$$\mathrm{Id} = \mathrm{Q_i}(\mathrm{x_0}) \times (\mathrm{vxo}) \times (\mathrm{Fsat})\mathrm{W}, \tag{1}$$

Where $\mathbf{Q_i(x_0)}$ and **vxo** are the channel charge density and velocity, respectively, at the VS point. **vxo** is assumed to be independent of bias voltages and is extracted from experimental data (Liu, Luisier et al. 2012). The VS charge density used for current computation (**Qinv_corr**) is slightly different than that used for charge computation (**Qinv**). This was done to smoothen the second derivative of **Id** with respect to **Vds** around **Vds** = 0 V.

The transition function **Fsat** is given as

$$\mathrm{Fsat} = \frac{\mathrm{Vdsi/Vdsat}}{\left(1 + \left(\frac{\mathrm{Vdsi}}{\mathrm{Vdsat}}\right)^{\beta}\right)^{\frac{1}{\beta}}} \tag{2}$$

where **Vdsat** is the saturation voltage given as

$$\text{Vdsat} = \text{Vdsats}(1 - \text{FF}) + \text{phit}\times\text{FF} \tag{3a}$$

$$\text{Vdsats} = \text{vxo}\times\frac{\text{Leff}}{\text{mu}} \tag{3b}$$

$$\text{FF} = \frac{1}{1 + \exp\left(\frac{\text{Vgscorr} - \text{Vtp}}{\text{aphit}}\right)} \tag{3c}$$

$$\text{Vtp} = \text{Vt0bs} - \text{delta}\times\text{Vdsi} - 0.5\text{aphit} \tag{3d}$$

$$\text{Vt0bs} = \text{Vt0} + \text{gamma}\times\left(\sqrt{\{\text{phib} - \text{Vbscorr}\}} - \sqrt{\{\text{phib}\}}\right) \tag{3e}$$

where the factors **Vgscorr** and **Vbscorr** are explained later. The term **aphit** = **alpha**×**phit** and **nphit** = **n**×**phit**, and other variables are explained in Table I. **phit** = **k**×**Tjun/q** is the thermal voltage, where k is the Boltzmann constant and q is the electronic charge. The term **FF** is used for Fermi function.

In the next sub-sections, equations pertaining to the computation of **Qinv_corr**, **Vgscorr**, and **Vbscorr** are explained.

Computation of Qinv_corr

$$\text{Qinv\_corr} = \text{Qref}\times\ln(1 + \exp(\text{eta})) \tag{4a}$$

$$\text{Qref} = \text{Cg}\times\text{nphit} \tag{4b}$$

$$\text{n} = \text{n0} + \text{nd}\times\text{Vdsi} \tag{4c}$$

$$\text{eta} = \frac{\text{Vgscorr} - (\text{Vt0bs} - \text{delta}\times\text{Vdsi} - \text{aphit}\times\text{FF})}{\text{nphit}} \tag{4d}$$

Where **Vt0bs** and **FF** are given as in Eq. (3c)-(3e).

Computation of Vgscorr and Vbscorr

$$\mathrm{Vgscorr} = \mathrm{Vgsi} + \mathrm{Vcorr}, \tag{5a}$$

$$\mathrm{Vbscorr} = \mathrm{Vbsi} + \mathrm{Vcorr} \tag{5b}$$

$$\mathrm{Vcorr} = \frac{(1 + 2\times\mathrm{delta})\mathrm{ab}}{2}\exp\left(-\frac{\mathrm{Vdsi}}{\mathrm{ab}}\right) \tag{5c}$$

$$\mathrm{ab} = 2(1 - 0.99\mathrm{FFpre})\mathrm{phit} \tag{5d}$$

$$\mathrm{FFpre} = \frac{1}{\left(1 + \exp\left(\frac{\mathrm{Vgs} - \mathrm{Vtpcorr}}{1.5\times\mathrm{aphit}}\right)\right)} \tag{5e}$$

$$\mathrm{Vtpcorr} = \mathrm{Vt0} + \mathrm{gamma}\left(\sqrt{\{\mathrm{phib} - \mathrm{Vbs}\}} - \sqrt{\{\mathrm{phib}\}}\right) \tag{5f}$$

Note that the correction factor **Vcorr** is computed from external **Vgs** and **Vbs** but internal **Vdsi**.

The impact of access-region resistances on current computation is modeled as

$$\mathrm{I(d,di)} = \frac{\mathrm{V(d)} - \mathrm{V(di)}}{\mathrm{Rd}} \tag{6a}$$

$$\mathrm{I(s,si)} = \frac{\mathrm{V(s)} - \mathrm{V(si)}}{\mathrm{Rs}} \tag{6b}$$

where **I(d,di)** is the current flow between terminals **d** and **di**, **I(s,si)** is the current flow between terminals **s** and **si**, **Rd = Rd0/W** and **Rs=Rs0/W**.

Equations (1)-(6) determine the transport in the channel.

Terminal Charges

For dynamic operation, the channel charge behavior must be accounted for in the device model. The time-dependent variation in the channel charge is supplied by displacement currents through the device terminals (Tsividis 1999) that, obviously, cannot be predicted by the static transport theory. The intrinsic charges associated with each terminal are computed self consistently with the transport model. The model terminal charges can produce the full matrix of capacitive components and their voltage dependences. The partitioning of charges at the source terminal (Qs) and the drain terminal (Qd) is accomplished through the Ward-Dutton charge-partitioning scheme (Ward 1981) that is universally true as long as the device operates under quasi-static conditions.

$$Qs = W\int_0^{Leff}\left(1-\frac{x}{Leff}\right)Qi(x)dx \tag{7a}$$

$$Qd = W\int_0^{Leff}\frac{x}{Leff}\,Qi(x)dx \tag{7b}$$

Where Qi(x) is the position-dependent inversion charge density along the channel.

Ballistic charges (parabolic profile)

To compute Qi(x) in ballistic transport regime, current continuity and energy balance are used along the channel. Using a parabolic potential profile along the channel, the charge Qi(x) is given as

$$Qi(x) = \frac{Qinv}{\sqrt{1+k\left(\frac{x}{Leff}\right)^2}} \tag{8a}$$

$$k = \frac{2qe}{me}\frac{Vdsi}{vxo^2} \tag{8b}$$

To compute terminal charges, **Qinv**, will be used instead of **Qinv_corr** that is used in computation of current. **Qinv** is computed from the same set of equations as 4(a)-4(d) but with **Vgscorr** replaced with **Vgsi**, **Vbscorr** replaced with **Vbsi**. **Qinv** is given as

$$\mathrm{Qinv} = \mathrm{Qref} \times \ln\left(1 + \exp\left(\frac{\mathrm{Vgsi} - (\mathrm{Vt0bs0} - \mathrm{delta} \times \mathrm{Vdsi} - \mathrm{aphit} \times \mathrm{FFpre})}{\mathrm{nphit}}\right)\right), \quad (9a)$$

$$\mathrm{Vt0bs0} = \mathrm{Vt0} + \mathrm{gamma} \times \left(\sqrt{\{\mathrm{phib} - \mathrm{Vbsi}\}} - \sqrt{\{\mathrm{phib}\}}\right) \quad (9b)$$

Using Eq. (8a) and (8b) in (7a) and (7b) and carrying out the integration,

$$\mathrm{qsb} = \mathrm{Qinv} \times \left(\frac{\sinh \mathrm{kq}}{\mathrm{kq}} - \frac{\sqrt{\{\mathrm{kq2} + 1\}} - 1}{\mathrm{kq2}}\right) \quad (10a)$$

$$\mathrm{qdb} = \mathrm{Qinv} \times \frac{\sqrt{\{\mathrm{kq2} + 1\}} - 1}{\mathrm{kq2}} \quad (10b)$$

$$\mathrm{kq} = \sqrt{\frac{\frac{2\mathrm{qe}}{\mathrm{me}}\mathrm{Vdsi}}{\mathrm{vxo}^2}} \quad (10c)$$

$$\mathrm{kq2} = \mathrm{kq} \times \mathrm{kq} \quad (10d)$$

Ballistic charges (linear potential profile)

If the potential profile in the channel is linear rather than parabolic, following equations must be used:

$$\mathrm{Qi(x)} = \frac{\mathrm{Qinv}}{\sqrt{1 + \mathrm{k}\left(\frac{\mathrm{x}}{\mathrm{Leff}}\right)}} \quad (11a)$$

$$\mathrm{qsb} = \mathrm{Qinv} \times \frac{(4\mathrm{k} + 4)\sqrt{\mathrm{k} + 1} - (6\mathrm{k} + 4)}{3\mathrm{k}^2} \quad (11b)$$

$$\mathrm{qdb} = \mathrm{Qinv} \times \frac{(2\mathrm{k} - 4)\sqrt{\mathrm{k} + 1} + 4}{3\mathrm{k}^2} \quad (11c)$$

In this version of the model, we have only implemented charges corresponding to the parabolic potential profile in the channel (Eq. (10a)-(10d)).

Drift-diffusion non-velocity saturated (DD-NVSAT) charges

In the non-saturation region of operation, V_{ds} is generally small, and the potential profile in the channel is wider and flatter than in saturation conditions. Under such conditions, carrier transport approaches drift/diffusion conditions dominated by mobility, as opposed to velocity for operation in saturation. The charges in the DD-NVSAT regime are given as (Tsividis 1999). Here **psis** denotes the surface potential solution in weak inversion.

$$qsc = Qinv \times \frac{6 + 12x + 8x^2 + 4x^3}{15(1+x)^2} \tag{12a}$$

$$qdc = Qinv \times \frac{4 + 8x + 12x^2 + 6x^3}{15(1+x)^2} \tag{12b}$$

$$x = 1 - Fsatq \tag{12c}$$

$$Fsatq = \frac{Vdsi/Vdsatq}{\left(1 + \left(\frac{Vdsi}{Vdsatq}\right)^{\beta}\right)^{\frac{1}{\beta}}} \tag{12d}$$

$$Vdsatq = \sqrt{FF0 \times aphit^2 + Vgta^2} \tag{12e}$$

$$FF0 = \frac{1}{1 + \exp\left(\frac{Vgsi - Vtp0}{aphit}\right)} \tag{12f}$$

$$Vtp0 = Vt0 + gamma \times \left(\sqrt{phib - Vbsi} - \sqrt{phib}\right) - delta \times Vdsi - 0.5aphit \tag{12g}$$

$$Vgta = \frac{1}{a}\frac{Qinv}{Cg} \tag{12h}$$

$$a = 1 + \frac{gamma}{2\sqrt{psis - Vbsi}} \tag{12i}$$

$$psis = phib + \frac{1 - gamma}{1 + gamma} + phit \times (1 + \ln(eta0)) \tag{12j}$$

$$eta0 = \frac{Vgsi - (Vt0bs0 - delta \times Vdsi - aphit \times FF)}{nphit} \tag{12k}$$

$$Vt0bs0 = Vt0 + gamma \times \left(\sqrt{\{phib - Vbsi\}} - \sqrt{\{phib\}}\right) \tag{12l}$$

Drain-induced barrier lowering (DIBL) correction to charges

$$\mathrm{qd} = \mathrm{qd} - \mathrm{dibl\_corr} \tag{13a}$$

$$\mathrm{dibl\_corr} = (1 - \mathrm{FF0})(1 - \mathrm{Fsatq}) \times \mathrm{qi} \times \mathrm{dQinv} \tag{13b}$$

$$\mathrm{dQinv} = \mathrm{Qinv} - \mathrm{Qinvi} \tag{13c}$$

$$\mathrm{Qinvi} = \mathrm{Qref} \times \ln(1 + \exp(\mathrm{etai})) \tag{13d}$$

$$\mathrm{etai} = \left(\frac{\mathrm{Vgsi} - (\mathrm{Vt0bs0} - \mathrm{aphit} \times \mathrm{FF})}{\mathrm{nphit}} \right) \tag{13e}$$

$$\mathrm{qi} = \mathrm{qsc} + \mathrm{qdc} \tag{13f}$$

Combining DD-NVSAT and ballistic charges

The function Fsat^2 is used to blend the DD-NVSAT and ballistic charges according to

$$\mathrm{qs} = \mathrm{qsc}(1 - \mathrm{Fsatq})^2 + \mathrm{qsb} \times \mathrm{Fsatq}^2 \tag{14a}$$

$$\mathrm{qd} = \mathrm{qdc}(1 - \mathrm{Fsatq})^2 + \mathrm{qdb} \times \mathrm{Fsatq}^2 \tag{14b}$$

The inversion charge partitioning into terminals **s** and **d** is given as

$$\mathrm{Qinvs} = \mathrm{tipe} \times \mathrm{Leff} \frac{\big((1 + \mathrm{dir})\mathrm{qs} + (1 - \mathrm{dir})\mathrm{qd}\big)}{2} \tag{15a}$$

$$\mathrm{Qinvd} = \mathrm{tipe} \times \mathrm{Leff} \frac{\big((1 - \mathrm{dir})\mathrm{qs} + (1 + \mathrm{dir})\mathrm{qd}\big)}{2} \tag{15b}$$

In the current implementation of the model, only DD-NVSAT charge model is selected when **CTM_select** = 1 else blended DD-NVSAT and ballistic charge model is selected.

Outer-fringing and inner-fringing charges

Outer fringing charges at the **s** and **d** terminals are given as

$$\mathrm{Qsov} = \mathrm{Cofs}\big(\mathrm{V(g)} - \mathrm{V(si)}\big) \tag{16a}$$

$$\mathrm{Qdov} = \mathrm{Cofd}\big(\mathrm{V(g)} - \mathrm{V(di)}\big) \tag{16b}$$

Inner-fringing charges are given as

$$\mathrm{Qsif} = \mathrm{tipe}\times\mathrm{Cif}\times\mathrm{FFx} \tag{17a}$$

$$\mathrm{Qdif} = \mathrm{tipe}\times\mathrm{Cif}\times\mathrm{FFy} \tag{17b}$$

$$\mathrm{FFx} = \mathrm{Vgsraw} - \mathrm{nphit}\times\mathrm{FSarg} \tag{17c}$$

$$\mathrm{FFy} = \mathrm{Vgdraw} - \mathrm{nphit}\times\mathrm{Fdarg} \tag{17d}$$

$$\mathrm{FSarg} = \frac{\mathrm{Vgsraw} - (\mathrm{Vt0x} - \mathrm{delta}\times\mathrm{Vdsi}\times\mathrm{Fsat}) + 0.5\mathrm{aphit}}{1.1\mathrm{nphit}} \tag{17e}$$

$$\mathrm{FDarg} = \frac{\mathrm{Vgdraw} - (\mathrm{Vt0y} - \mathrm{delta}\times\mathrm{Vdsi}\times\mathrm{Fsat}) + 0.5\mathrm{aphit}}{1.1\mathrm{nphit}} \tag{17f}$$

$$\mathrm{Vt0x} = \mathrm{Vt0} + \mathrm{gamma}\left(\sqrt{\mathrm{phib} - \mathrm{tipe} * \left(\mathrm{V(b)} - \mathrm{V(si)}\right)} - \sqrt{\mathrm{phib}}\right) \tag{17g}$$

$$\mathrm{Vt0y} = \mathrm{Vt0} + \mathrm{gamma}\left(\sqrt{\mathrm{phib} - \mathrm{tipe} * \left(\mathrm{V(b)} - \mathrm{V(di)}\right)} - \sqrt{\mathrm{phib}}\right) \tag{17h}$$

Body charge

The body charge is given as

$$\mathrm{Qb} = \mathrm{tipe}\times\mathrm{W}\times\mathrm{Leff}\times\left(\mathrm{Cg}\times\mathrm{gamma}\sqrt{\mathrm{psis} - \mathrm{Vbsi}} + \frac{\mathrm{a}-1}{\mathrm{a}}\right)\mathrm{Qinv} \times(1 - \mathrm{qi}) \tag{18}$$

Where **psis** is given in Eq. (12j), **a** is given in Eq. (12i) and **qi** is given in Eq. (13f).

Net-charge/capacitance model

All the charges are combined to give partitioned charges at **s** and **d** terminals according to

$$Qs = -W(Qinvs + Qsov + Qsif) \tag{19a}$$

$$Qd = -W(Qinvd + Qdov + Qdif) \tag{19b}$$

$$Qg = -(Qs + Qb + Qd) \tag{19c}$$

The inter-nodal capacitance between terminals i and j is given as

$$Cij = -\frac{\partial Qi}{\partial Vj} \text{ if } i \neq j \tag{20a}$$

$$Cii = \frac{\partial Qi}{\partial Vi} \tag{20b}$$

Once the nodal charges are obtained, the inter-nodal capacitances can be evaluated using expressions given in Eq. (20a) and (20b).

Parameter extraction

A total of seven parameters are optimized as highlighted in Table I, while other parameters are obtained from experimental details on the device. Table II gives the list of parameters with their initial guess and lower and upper bounds that are hard-coded in the extraction routine.

Parameter	Lower bound	Upper bound	Initial guess
Rs0 = Rd0 [Ω.μm]	0	1000	100
delta (DIBL) [V/V]	0	0.5	0.15
n0 [unit-less]	1.0	2.0	1.34
nd [V^{-1}]	0	0.5	0
vxo [cm/s]	10^6	10^8	1.2×10^7
mu [cm^2/Vs]	50	1000	200
Vt0 [V]	0.2	0.8	0.4

Above numbers are hard-coded in the extraction routine and it is recommended that they not be tweaked to guarantee the convergence of the code.

There are three files that are related with parameter extraction:
extract_main.m
optimize_transfer.m
optimize_output.m

Setting up the files for extraction routine

extract_main.m contains the extraction routine that calls two other files: ***extract_transfer.m*** and ***extract_output.m*** files. Two experimental data sets are considered: 32-nm and 45-nm from Intel (Packan 2009; Wei, Mysore et al. 2012). To choose a particular data set, uncomment lines in ***extract_main.m*** corresponding to the appropriate experimental data set. **UNCOMMENT** flag has been added as comments in *extract_main.m* file for the following:

a) Physical dimensions that are fixed (W, Lgdr, dLg) and gate capacitance (Cg).
b) Output file name that stores the values of extracted parameters (*output_text_32nm.txt* OR *output_text_45nm.txt*).
c) Plotting appropriate output and transfer curves by choosing the correct data set.

In addition to the above changes in ***extract_main.m***, files ***optimize_transfer.m*** and ***optimize_output.m*** need to have appropriate experimental data file names. UNCOMMENT flag has been added as comments to both the optimization files. That is,

a) Choose appropriate file name (*idvg_Intel_32_nFET_09* OR *idvg_Intel_45_nFET_12.txt*) in ***optimize_transfer.m***
b) Choose appropriate file name (*idvd_Intel_32_nFET_09* OR *idvd_Intel_45_nFET_12.txt*) in ***optimize_output.m***

By default, extract_main.m routine runs for the 45-nm experimental data set. Hence, to generate results for 32-nm experimental data set, user needs to make the changes mentioned above in the three files.

Input file format

Input file must be provided in the format shown in Figure 3.

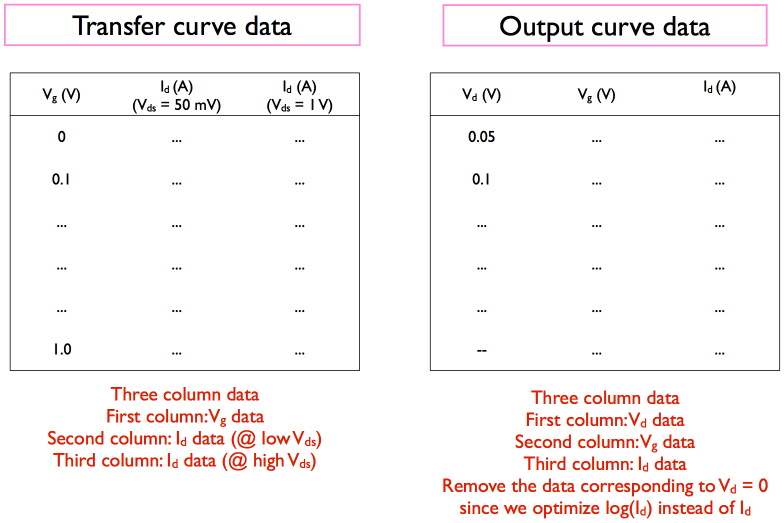

Figure 3: Input-file format to be provided in the extraction routine.

Optimization routine

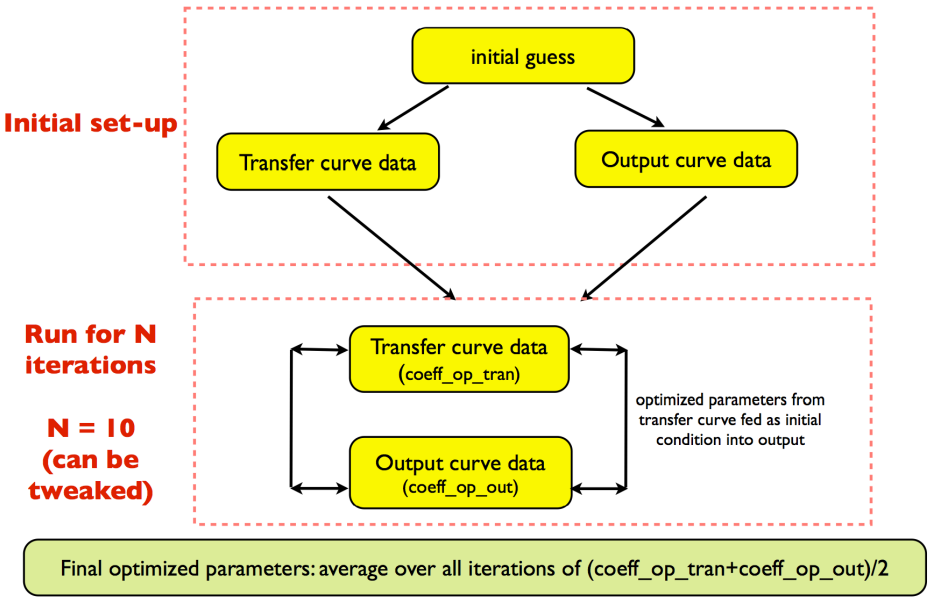

Figure 4: Optimization routine for extracting parameters based upon transfer and output data for the transistor.

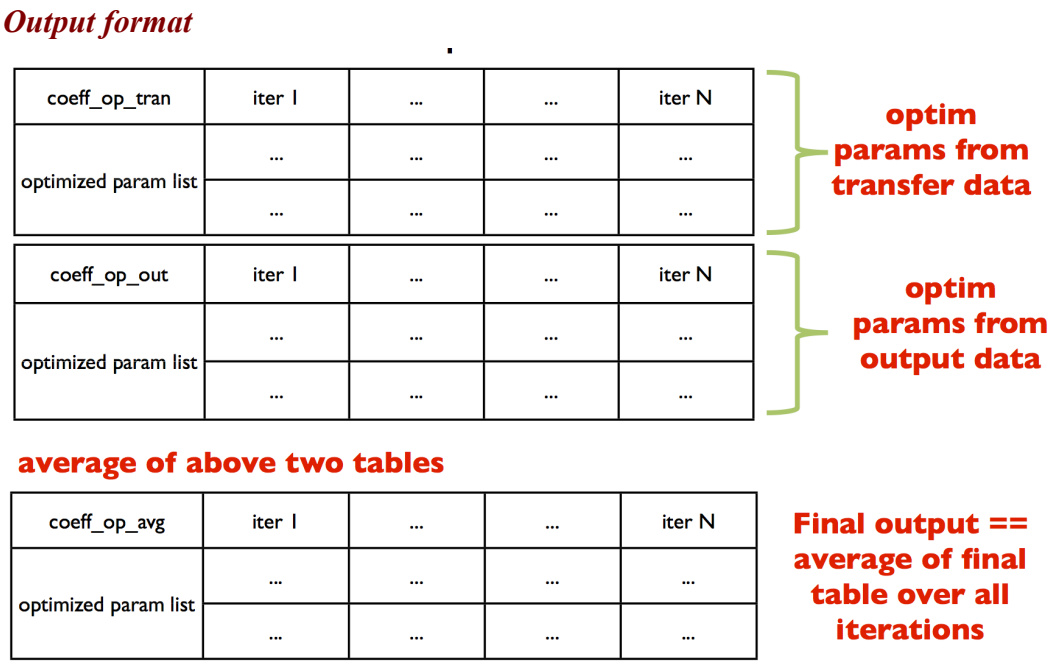

Figure 5: The average over all iterations gives the final optimized parameters.

Simulation Results (using parameter extraction tool)

Next we present simulation results from two experimental data sets (Lgdr = 32 nm (Packan 2009) and 45 nm (Wei, Mysore et al. 2012) from Intel). Following tables shows the extracted parameters for the two data sets (blue values indicate extracted parameters).

Table III: Lgdr = 32 nm

Parameter	Value
W	1 µm
Lgdr	32 nm
dLg	9 nm
Cg	2.57×10^{-6} F/cm^2
beta	1.8
alpha	3.5
Rs0 = Rd0	**61 Ω.µm**
delta	**0.087 V/V**
n0	**1.55**
nd	**0.3942 V^{-1}**
vxo	**1.53×10^7 cm/s**
mu	**181 cm^2/Vs**
Vt0	**0.5174 V**

Table IV: Lgdr = 45 nm

Parameter	Value
W	1 µm
Lgdr	45 nm
dLg	7.56 nm
Cg	2.55×10^{-6} F/cm^2
beta	1.8
alpha	3.5
Rs0 = Rd0	**47.1 Ω.µm**
delta	**0.072 V/V**
n0	**1.54**
nd	**0.2959 V^{-1}**
vxo	**0.96×10^7 cm/s**
mu	**135 cm^2/Vs**
Vt0	**0.464 V**

Transfer characteristics

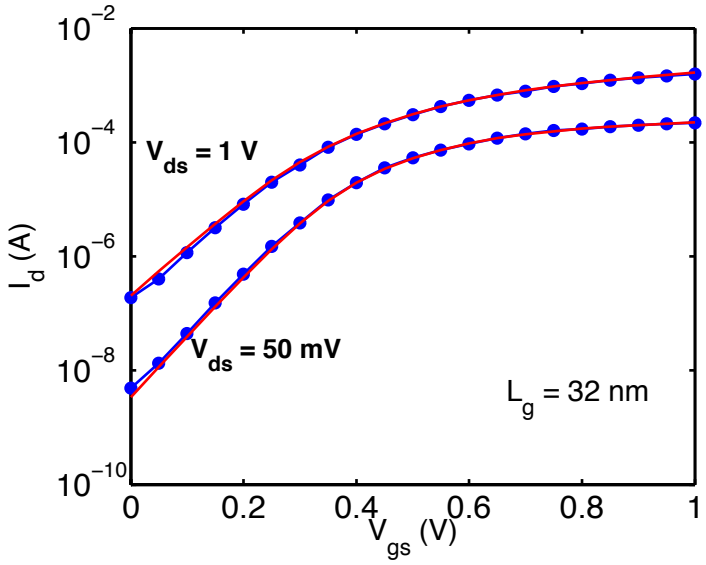

Figure 6: Transfer curve for Lgdr = 32 nm. Experimental data is shown in symbols, while the model fits are shown in solid lines.

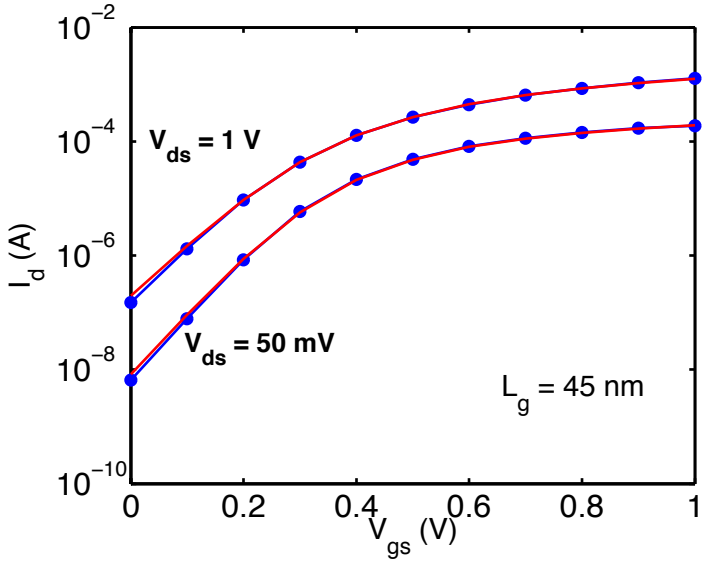

Figure 7: Transfer curve for Lgdr = 45 nm. Experimental data is shown in symbols, while the model fits are shown in solid lines.

Output characteristics

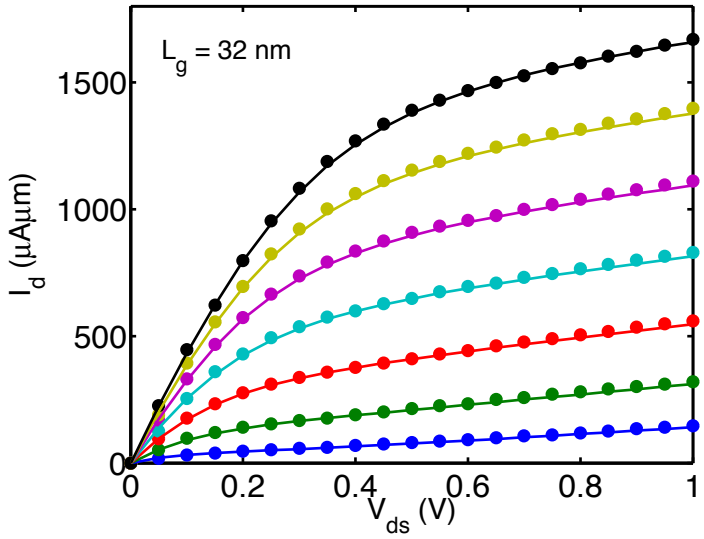

Figure 8: Output curve for Lgdr = 32 nm. Experimental data is shown in symbols, while the model fits are shown in solid lines. Vgs ranges from 0.4V to 1.0V in steps of 0.1V from bottom to top curves.

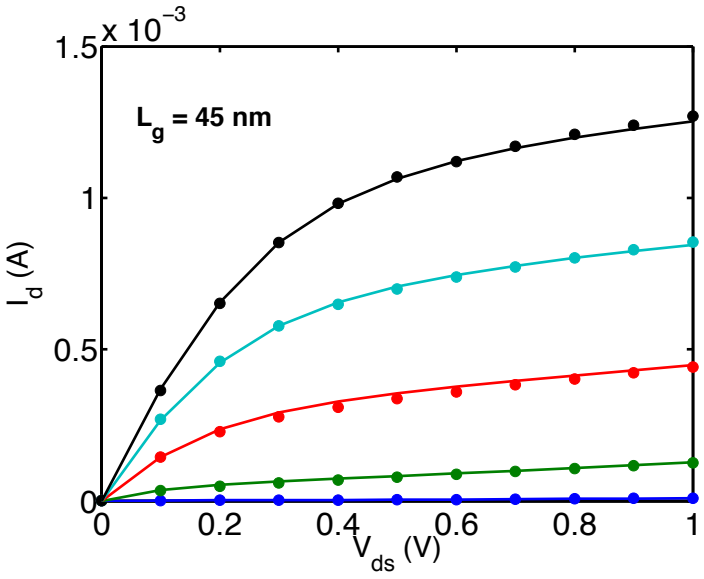

Figure 9: Output curve for Lgdr = 45 nm. Experimental data is shown in symbols, while the model fits are shown in solid lines. Vgs value ranges from 0.2V to 1.0V in steps of 0.2V from bottom to top curves.

Model exerciser

To run the model exerciser with appropriate experimental data set, UNCOMMENT lines for 32-nm or 45-nm data sets. UNCOMMENT flag has been added as a comment in *model_exerciser.m* file.

Simulation Results (using model_exerciser.m file)

1st Derivative and 2nd derivative of current with respect to Vds

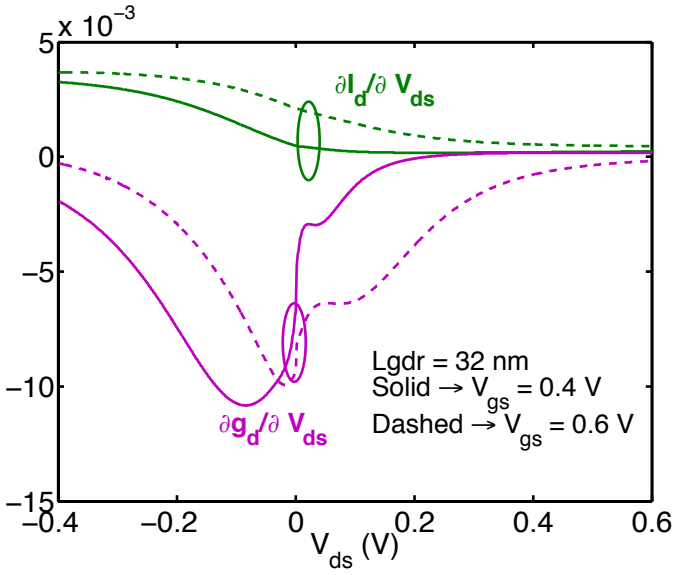

Figure 10: 1st and 2nd derivative of current with respect to Vds for two values of Vgs: (i) Vgs = 0.4 V (below threshold voltage) and (ii) Vgs = 0.6 V (above threshold voltage). The third derivative of current is not continuous at Vds=0V.

Charges with respect to Vds

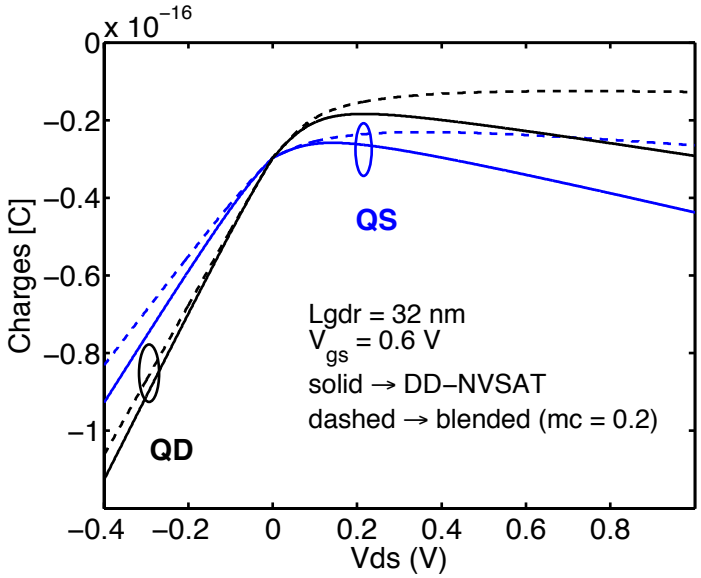

Figure 11: Charges with respect to Vds. Quasi-ballistic charges (mc = 0.2) are lower than the DD-NVSAT charges (CTM_select = 1).

Capacitances with respect to terminal voltages

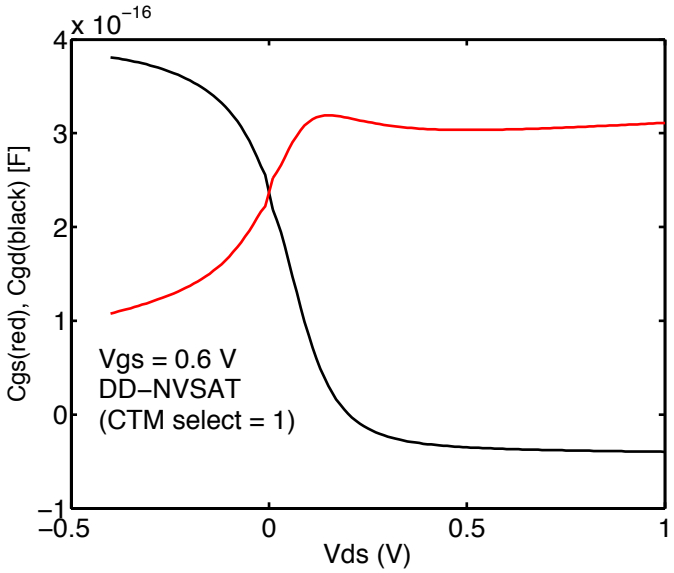

Figure 12: Capacitances, Cgs and Cgd, with respect to Vds using only the DD-NVSAT model (CTM_select = 1) for Lgdr = 32 nm device.

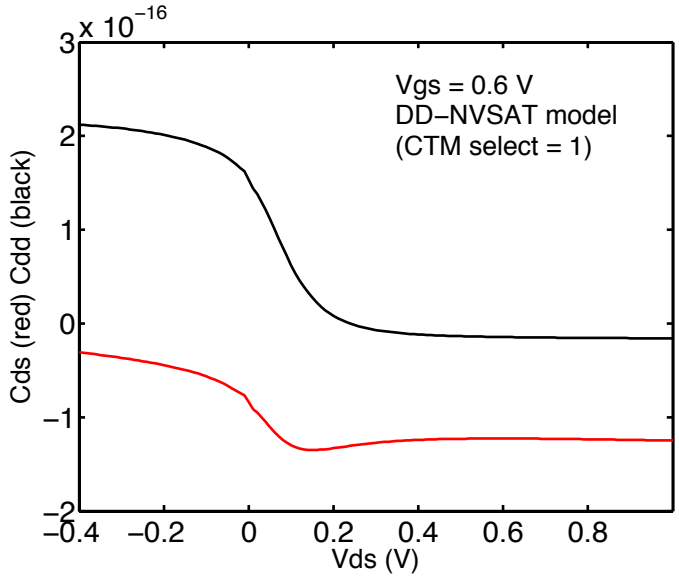

Figure 13: Capacitances, Cds and Cdd, with respect to Vds using only the DD-NVSAT model (CTM_select = 1) for Lgdr = 32 nm device.

Bibliography

Chan, M., K. Y. Hui, et al. (1998). "A robust and physical non-quasi-static transient AC and small-signal model for circuit simulation." IEEE Transactions on Electron Devices **45**(4): 834-841.

Jeong, C., D. A. Antoniadis, et al. (2009). "On backscattering mobility in nanoscale silicon MOSFETs." IEEE Transactions on Electron Devices **56**(11): 2762-2769.

Khakifirooz, A., O. M. Nayfeh, et al. (2009). "A Simple Semiempirical Short-Channel MOSFET Current–Voltage Model Continuous Across All Regions of Operation and Employing Only Physical Parameters." IEEE Transactions on Electron Devices **56**(8): 1674-1680.

Liu, Y., M. Luisier, et al. (2012). "On the Interpretation of Ballistic Injection Velocity in Deeply Scaled MOSFETs." IEEE Transactions on Electron Devices **59**(4): 994-1001.

Lundstrom, M. S. (2009). Fundamentals of carrier transport, Cambridge University Press.

Natori, K. (1994). "Ballistic metal-oxide-semiconductor field effect transistor." Journal of Applied Physics **76**(8): 4879-4890.

Packan, P. (2009). High performance 32nm logic technology featuring 2nd generation high-k + metal gate transistors. IEEE International Electron Devices Meeting (IEDM).

Rhew, J.-H., Z. Ren, et al. (2002). "A numerical study of ballistic transport in a nanoscale MOSFET." Solid State Electronics **46**(11): 1899-1906

Tsividis, Y. (1999). Operation and Modeling of the MOS Transistor. Boston, MA, McGraw-Hill.

Ward, D. E. (1981) Integrated Circuits Laboratory. **G201-10**,

Wei, L., O. Mysore, et al. (2012). "Virtual-source-based self-consistent current and charge FET models: from ballistic to drift-diffusion velocity-saturation operation." IEEE Transactions on Electron Devices **59**(5): 1263-1271.